# Cerebrospinal Fluid Leak Detection with a Carbon Nanotube-Based Field-Effect Transistor Biosensing Platform

Wenting Shao,<sup>†</sup> Galina V. Shurin,<sup>‡</sup> Xiaoyun He,<sup>†</sup> Zidao Zeng,<sup>†</sup> Michael R. Shurin<sup>‡</sup> and Alexander Star\*, <sup>†</sup>, §

† Department of Chemistry, University of Pittsburgh, Pittsburgh, Pennsylvania 15260, United States

<sup>‡</sup> Department of Pathology, University of Pittsburgh Medical Center, Pittsburgh, Pennsylvania 15260,

United States

§ Department of Bioengineering, University of Pittsburgh, Pittsburgh, Pennsylvania 15261, United

States

## **ABSTRACT**

Cerebrospinal fluid (CSF) leak may lead to life-threatening complications if not detected promptly. However, gel electrophoresis, the gold standard test for confirming CSF leak by detecting beta2-transferrin ( $\beta$ 2-Tf), requires 3-6 hours and is labor intensive. We developed a new  $\beta$ 2-Tf detection platform for rapid identification of CSF leak. The 3-step design, which includes two steps of affinity chromatography and a rapid sensing step using a semiconductor-enriched single-walled carbon nanotube field-effect transistor (FET) sensor, circumvented the lack of selectivity that anti-transferrin antibody exhibits for transferrin isoforms, and markedly shortened the detection time. Furthermore, three different sensing configurations for the FET sensor were investigated for obtaining the optimal  $\beta$ 2-Tf sensing results. Finally, body fluid (CSF and serum) tests employing our 3-step strategy demonstrated high sensitivity, suggesting its potential to be used as a rapid diagnostic tool for CSF leak.

Keywords: neurosurgery, beta2-transferrin, diagnostic test, antibody, graphene, biosensor

#### 1. INTRODUCTION

Leakage of cerebrospinal fluid (CSF) is a serious condition that can result from trauma, invasive tumors, congenital malformation, or surgical procedures and results in significant morbidity and mortality if left untreated. Without appropriate treatment, CSF leaks can lead to life-threatening cases of meningitis, intracranial hypotension, or pneumocephalus. Identification of CSF in non-native sites requires immediate surgical intervention, usually in the form of endoscopic endonasal or transcranial surgery. However, the diagnosis of CSF leak is often difficult to confirm. Traditional chemical analyses of biological fluids (e.g., glucose, total protein, specific gravity) are unreliable and have been largely abandoned. Radiographic and magnetic imaging methods, especially those involving the injection of dyes or radiographic agents, are not always successful, require expensive, time-consuming procedures, and may introduce additional risks to the patient. Accumulating clinical data do not support the use of the ring sign, glucose testing, radionuclide cisternography, or computed tomography cisternography for identification of CSF leak.

Clinical laboratory detection of CSF leak takes advantage of the heterogeneity of transferrins in bodily fluids and utilizes beta2-transferrin ( $\beta$ 2-Tf) detection in available specimens as an indicator of CSF presence.<sup>4</sup> Transferrin is a 79 kDa iron-binding protein transporting and maintaining iron homeostasis.<sup>5</sup> The number of sialic acid groups varies to create 9 transferrin isoforms ranging from 0 to 8 sialic acid groups.<sup>6</sup> The major isoform with 4 sialic acid groups is  $\beta$ 1-transferrin, the predominant form in most body fluids including serum. In contrast,  $\beta$ 2-Tf (carbohydrate-free, desialated), is formed by loss of sialic acid due to the presence of neuraminidase in the central nervous system (CNS) and is confined to the CSF, aqueous humor, and perilymph.<sup>7-8</sup> Thus,  $\beta$ 2-Tf is a CSF-specific variant of transferrin used as an endogenous marker of CSF leakage if detected in nasal or aural fluid.  $\beta$ 2-Tf can be resolved from the other isoforms of transferrin because differences in sialic acid content change the isoelectric point of

the protein, allowing separation by gel electrophoresis. <sup>9-10</sup> However, the main problem with electrophoretic separation of transferrins and their staining is a running time required for electrophoresis + transfer + Western blot: 3 to 6 h, which is not always adequate for the β2-TF assay when ordered on STAT turnaround time priority level (from the Latin *statim* - immediately or without delay) by neurosurgeons. Another problem is the result interpretation which requires a pathologist or a highly trained and experience medical technologist who are not always available for STAT procedures.

Nanomaterial-based biosensors have shown great potential in diagnostic tools as they offer high sensitivity, label-free and rapid detection of biomolecules as well as easy fabrication and miniaturization. 11-17 In particular, CNT-based field-effect transistor (FET) biosensors are promising candidates for point-of-care diagnostic devices, owing to the outstanding electronic and mechanical properties of CNTs. 18-20 CNT-based FET biosensors probe the interactions of biomolecules with the semiconducting (sc-) single-walled carbon nanotube (SWCNT) channel causing alteration in the electrical conductance of the sc-SWCNTs. Therefore, high-purity sc-SWCNTs, which enable high on-state conductance and high on/off ratio for FETs, are ideal material in order to develop high-performance FET devices. 21-23 Recently, high-purity sc-SWCNTs have shown promise for sensing applications, such as gas sensors, 24-27 humidity monitor, 28 infrared imaging sensor, 29 as well as ultrasensitive biosensors, such as aptasensors, 30-32 DNA detection 33 and label-free protein sensors. 34-36

Herein, we present a new  $\beta$ 2-Tf laboratory detection method for different biological fluids with high sensitivity, short turnaround time (around 1 hour) and easy instrument access. The 3-step strategy for  $\beta$ 2-Tf detection includes two steps of affinity chromatography to isolate  $\beta$ 2-Tf and a rapid  $\beta$ 2-Tf sensing step utilizing a high-purity sc-SWCNT FET device. Three different sensing configurations for the sc-SWCNT FET sensor were investigated for obtaining the optimal  $\beta$ 2-Tf sensing results. Finally,  $\beta$ 2-Tf detection in body fluids, namely CSF and serum,

employing the 3-step strategy demonstrated markedly improvement in the sensitivity and responsiveness than the gold standard electrophoresis method, indicating a proof-of-principle for use as a rapid CSF leak diagnostic tool. We therefore anticipate providing a more affordable, fast and point-of-care compatible methodology for  $\beta$ 2-TF analysis in human clinical specimens.

#### 2. EXPERIMENTAL SECTION

2.1 Enzyme-linked immunosorbent assay (ELISA). Transferrin human ELISA kit was purchased from Thermofisher Scientific (Cat#: EHTF). For the standard curve, transferrin standards at concentrations of 0.1 ng/mL, 1 ng/mL, 10 ng/mL, 100 ng/mL, 500 ng/mL, 1 μg/mL and 10 μg/mL were prepared using recombinant human serum transferrin (MilliporeSigma, Cat#: T8158). A 2 mg/mL recombinant human serum transferrin solution mixed with 10 mg/mL BSA in PBS was treated with neuraminidase (MilliporeSigma, Cat#: N7885) and used as the positive sample. The same solution without the neuraminidase treatment was used as the negative sample. Both positive and negative samples were run through the two steps of separation using Tf-ab functionalized and serotonin functionalized affinity columns. The eluate from step 2 was collected for ELISA test.

ELISA was performed following the instruction provided with the kit. Absorbance was measured at both 450 nm and 550 nm (as background) using a Tecan M1000 pro plate reader. For data analysis, background was subtracted from all samples measured. The standard curves were run twice to determine the intra-assay precision. Both positive and negative samples were run twice, and the blank was run 5 times. All data reported in the figure and table were Mean  $\pm$  SD.

Affinity column preparation. Anti-transferrin antibody functionalized column was prepared by immobilizing anti-transferrin antibody (Tf-ab, Fisher Scientific, Cat#: PA184854) on CNBr-activated Sepharose® 4B (MilliporeSigma, Cat#: C9142) according to manufacturer's

instructions. Briefly, 25 mg of lyophilized CNBr-Sepharose were suspended in 1 mM HCl in a spin column (Thermo Fisher Scientific, Cat#: 69725), pH 3.0 and subsequently washed with 1 mM HCl for 15 min. Tf-ab was diluted 10-fold in coupling buffer (0.1 M NaHCO<sub>3</sub>, 0.5 M NaCl, pH 8.3), mixed with Sepharose (1 mg of Tf-ab per mg of Sepharose 4B) and incubated at room temperature for 2 h. After incubation, excess ligand was washed away with coupling buffer by centrifugation. The suspension was then incubated with 300 μL of 1 M ethanolamine, pH 8.0 for 2 h at room temperature in order to block any remaining active groups. After blocking, the material was washed with three cycles of alternating pH (0.1 M sodium acetate, 0.5 M NaCl, pH 4.0 and coupling buffer, pH 8.0). The final product was then washed with 300 μL nanopure water and stored in 0.5 M NaCl at 4°C.

Serotonin (MilliporeSigma, Cat#: H9523) was immobilized via its amine on CNBr-Sepharose by the cyanogen bromide method, similar to Tf-ab functionalization. Briefly, 25 mg of lyophilized CNBr-Sepharose were suspended in 1 mM HCl, pH 3.0 and subsequently washed with 1 mM HCl for 15 min. 40 mg serotonin-HCl were dissolved in 10 mL coupling buffer (0.1 M NaHCO<sub>3</sub>, 0.5 M NaCl, pH 8.3) and added to the activated CNBr-Sepharose in a spin column and incubated for 2 h at room temperature with light protection. Following, excess ligands were washed away, and the remaining active groups were blocked using 1 M ethanolamine, pH 8.0 for 2 h at room temperature. After blocking, the column was washed with three cycles of alternating pH, and then equilibrated in 0.5 M NaCl for storage at 4 °C.

Affinity chromatography. CSF (Thermo Fisher Scientific, Cat#: 50-203-6082) and serum (Thermo Fisher Scientific, Cat#: BP2657100) samples were used as a positive and a negative control. Serum samples were diluted 100-fold with 1× phosphate buffered saline (PBS) prior to chromatography steps. CSF samples had no pretreatments.

In step 1, 200  $\mu$ L of CSF (or 100-fold diluted serum) sample was loaded onto the Tf-ab functionalized column and incubated for 20 min at room temperature before centrifugation at

 $10,000 \times g$  for 2 min for elution. The bound total transferrin was eluted from Tf-ab/Sepharose column by applying the stripping buffer (0.1 M Glycine HCl, pH = 2.6, 200 µL each time) twice. The pH of the eluate was recovered immediately by adding 1 M Tris (pH 8.3) and loaded to the serotonin functionalized column for step 2. After a 20 min incubation at room temperature, the column was centrifuged at  $10,000 \times g$  for 2 min and the eluate was collected for  $\beta$ 2-Tf detection in step 3. The column was then stripped with 500 mM sodium chloride in 20 mM sodium phosphate (pH = 6).

**2.2 Device fabrication.** High-purity semiconducting single-walled carbon nanotubes were obtained commercially (IsoSol-S100, Raymor Industries Inc.) and were prepared at 0.02 mg/mL in toluene. Interdigitated gold electrodes (channel length of 10 μm) were patterned on a Si/SiO<sub>2</sub> substrate using photolithography. SWCNTs were then deposited between gold electrodes via dielectrophoresis (DEP) with an AC frequency of 100 kHz, applied bias voltage of 10 V, and bias duration of 120 s.

Anti-transferrin antibody (Tf-ab) functionalization on SWCNTs was achieved via 1-ethyl-3-(3-dimethylaminopropyl)carbodiimide hydrochloride (EDC)/N-hydroxysulfo-succinimide (sulfo-NHS) coupling. The SWCNT FET devices were first activated in 100  $\mu$ L of EDC/sulfo-NHS solution (50 mM/50 mM in 1× PBS, pH = 5.5) followed by a rinse with nanopure water. The devices were then incubated with 10  $\mu$ L of 100  $\mu$ g/mL Tf-ab (in 1× PBS) for 2 h at room temperature and rinsed thoroughly with nanopure water after incubation. To prevent nonspecific binding, the devices were soaked in a blocking buffer (0.1% Tween 20 and 4% polyethylene glycol in PBS) for 30 min to block unreacted surface.

FET measurements. FET characteristics of SWCNT FET devices were studied employing liquid-gated FET device configuration. Nanopure water was used as the gating electrolyte. Characteristic FET curves, i.e., source-drain conductance (G) versus gate voltage (V<sub>g</sub>), were

taken by sweeping the gate voltage from +0.6 to -0.6 V<sub>g</sub> versus a 1 M Ag/AgCl reference electrode with a fixed source-drain voltage of 50 mV.

A series of transferrin solutions ranging from  $10^{-4}$  fg/mL to 1 µg/mL were prepared using recombinant human serum transferrin (MilliporeSigma, Cat#: T8158). For transfer characteristic measurements using bare SWCNT and Tf-ab-SWCNT approach, the sc-SWCNT FET devices were first incubated in 10 µL of transferrin solution for 2 min, then rinsed with nanopure water, and measured in nanopure water as the gating electrolyte. For transfer characteristic measurements using Au electrode approach, the gold disk electrode (2 mm diameter) was first treated with gold surface cleaning solution (MilliporeSigma, Cat#: 667978), and then immersed in  $10 \mu$ L of transferrin solution for 2 min. Next, the Au electrode was washed with nanopure water and measured in nanopure water as the gate electrolyte. To remove the absorbed proteins on the gold surface after the measurements, the gold surface was rinsed with RIPA buffer (MilliporeSigma, Cat#: R0278) for 5 times and then sonicated in acetone for 30 min.

For body fluid tests, 10  $\mu$ L of the eluate from step 2 was added to the sc-SWCNT FET devices or the gold disk surface for incubation for 2 min followed by a rinse with nanopure water. All FET characteristics measurements were recorded in nanopure water as the gating electrolyte. The relative response (R) of each FET device was calculated using  $R = \Delta I_d/I_0$ , where  $\Delta I = |I_d-I_0|$ , and  $I_0$  is the drain current in nanopure water before transferrin exposure at  $-0.5~V_g$ . To construct the calibration curve, relative responses calculated from each device tested were averaged at each concentration and plotted against transferrin concentrations on a logarithmic scale. Error bars represented one standard error (SE). The number of devices (n) tested for each experiment was specified in the text.

- **2.3 Atomic force microscopy (AFM).** AFM images were recorded using Bruker multimode 8 AFM system with a Veeco Nanoscope IIIa controller in tapping mode. AFM images were processed in Gywddion.
- 2.4 Electrochemical impedance spectroscopy (EIS). All impedance measurements were performed using a CH Instruments electrochemical workstation (Instrument model: 7042C). Recombinant transferrin solutions were prepared from 1 fg/mL to 1  $\mu$ g/mL. For each concentration, 10  $\mu$ L of the transferrin solution was added on the gold disk surface at an increasing concentration order and incubated for 2 min, followed by a rinse with nanopure water. The impedance was measured in PBS solution with an AC amplitude of 5 mV over a frequency (f) range of 0.05 Hz to  $10^5$  Hz.

UV-vis-NIR absorption spectroscopy. 100  $\mu$ L of 0.02 mg/mL sc-SWCNTs were drop casted on a 1" × 1" quartz slide and heated at 200 °C to evaporate the solvent. UV-vis-NIR spectra of sc-SWCNT were collected using a Perkin-Elmer Lambda 900 UV-vis-NIR spectrophotometer.

**2.5 X-ray photoelectron spectroscopy.** Thermo ESCALAB 250 Xi XPS was used to generate X-ray photoelectron spectroscopy (XPS) data with monochromated Al Kα X-rays as the source. The spot size was 650-μm and the samples were charge-compensated using an electron flood gun.

Scanning electron microscopy. Scanning electron microscopy (SEM) was performed on a Si/SiO<sub>2</sub> chip using a ZEISS Sigma 500 VP instrument.

2.6 Fluorescence imaging. Fluorescence images were obtained using an Olympus 1X81/1X2-UCB microscope. For nonspecific binding of transferrin on sc-SWCNTs, 10 μL of 100 μg/mL Alexa Fluor 647 conjugated transferrin (Thermo Fisher Scientific, Cat#: T23366) was added to the sc-SWCNT device and incubated for 2 min at room temperature. Fluorescence images of bare sc-SWCNT devices before and after Alexa Fluor 647 conjugated transferrin binding were captured under excitation of 633 nm. For Tf-ab functionalized sc-SWCNT devices, Tf-

ab was functionalized on the sc-SWCNTs via EDC/NHS coupling. 10  $\mu$ L of 10  $\mu$ g/mL Alexa Fluor 546 conjugated anti-IgG secondary antibody (Thermo Fisher Scientific, Cat#: A11056) was then added to the device and incubated for 10 min at room temperature. As a control, 10  $\mu$ L of 10  $\mu$ g/mL Alexa Fluor 546 conjugated anti-IgG secondary antibody was also added to a bare sc-SWCNT FET device with blocking. All fluorescence images were taken under excitation of 532 nm.

Raman spectroscopy. Raman spectroscopy was performed on a XplorA Raman-AFM/TERS system. 785 nm (100 mW) excitation laser was used and operated at 1% power.

2.7 Gel electrophoresis and Western blot. Gel electrophoresis was carried out on a glass slide on 1% agarose (SeaKem® Agarose, Lonza) in a barbital buffer (MilliporeSigma, Cat#: B5934). Each sample (2 μL) was applied on the gel using a 6-lane template as the alignment guide. Excess sample was removed by gently blotting the template with a Whatman filter paper. The glass slide was placed inside the electrophoresis chamber (Horizontal Electrophoresis System, C.B.S. Scientific) with 4 trimmed pieces of blotter C paper (Helena) premoistened with barbital buffer on each side as a conduit for the buffer. The gel electrophoresis was run at 250 V for 1 hour in barbital buffer with a circulated cooling solution or cold water.

After electrophoresis, a 0.45-μm pore nitrocellulose membrane (GE Healthcare Life Sciences) moistened with deionized (DI) water was placed on top of the glass slide and pressed for 30 min with weights to transfer the protein from the gel to the membrane. The membrane was then blocked with 1% nonfat dry milk in BupH<sup>TM</sup> Tris buffered saline (ThermoFisher Scientific, Cat#: 28379) for 20 min, followed with rinses with DI water for 6-8 times. Next, the membrane was first incubated in a buffer with 1:2500 diluted goat anti-transferrin antibody (Cappel, catalog# 55139), 1% bovine serum albumin (BSA), 4% polyethylene glycol (PEG), and 0.05% Tween-20, Tris-buffered saline solution for 20 min. Then blots were rinsed with DI water 6-8 times, and incubated with 1:5000 diluted horseradish peroxidase-conjugated chicken anti-goat

IgG antibody (MilliporeSigma, Cat#: AP163P) in a 1% BSA, 4% PEG, and 0.05% Tween-20, Tris-buffered saline solution for 20 min. After another rinse with DI water for 6-8 times, the membrane was incubated in a 0.85% NaCl solution for 10 min and then developed in 3,3',5,5'-Tetramethylbenzidine (TMB) reagent (MilliporeSigma, Cat#: T0440). The membrane was washed 3 times with DI water when the development was finished.

#### 3. RESULTS AND DISCUSSION

Due to the lack of specific receptor for  $\beta$ 2-transferrin ( $\beta$ 2-Tf), separation steps were employed to first separate β2-Tf from a specimen in order for the detection on a sc-SWCNT FET sensor. Thus, here we present a 3-step design for  $\beta$ 2-Tf detection: 1) Isolation of all transferrin isoforms from other biological species present in the sample, 2) separation of β2-Tf from the other isoforms and 3)  $\beta$ 2-Tf detection with a SWCNT FET sensor (Figure 1). Both steps 1 and 2 are achieved by utilizing commercial affinity chromatography platform. In step 1, transferrin (all isoforms) was separated from other species using an anti-transferrin antibody (Tf-ab) immobilized Sepharose column. The bound transferrin was then stripped from the column and loaded into a serotonin (5-hydroxytryptamine) functionalized column (step 2) for the separation of β2-Tf. Serotonin is a sialic acid-binding molecule, which is nontoxic and commercially available at a relatively low price, making it suitable for clinical use.<sup>37</sup> Affinity of serotonin towards sialylated glycoproteins was proven<sup>38-39</sup> and since then it was used successfully for the analysis and purification of glycans, glycopeptides, and glycoproteins. The successful separation of β2-Tf using the 2-step separation approach was confirmed by enzyme-linked immunosorbent assay (ELISA), where transferrin was detected in eluate from step 2 from the positive sample, while no transferrin was detectable from the negative sample due to the absence of  $\beta$ 2-Tf in the original sample (Figure S1 and Table S1).



**Figure 1.** The 3-step strategy for detection of β2-Tf. Step 1, separation of all transferrin isoforms from the sample using anti-transferrin antibody functionalized affinity column. Step 2, separation of β2-Tf from other isoforms using serotonin functionalized affinity column. Step 3, detection of β2-Tf with a sc-SWCNT FET device. Insets show 3 different approaches for β2-Tf detection using a sc-SWCNT FET device, i.e., I. Bare SWCNTs: nonspecific binding of β2-Tf to bare sc-SWCNTs; II. Tf-ab-SWCNTs: detection of β2-Tf via anti-transferrin antibody functionalized sc-SWCNTs; III. Au electrode: detection of β2-Tf through binding to a gold gate electrode.

The β2-Tf FET sensing device was built utilizing high purity sc-SWCNTs as the sensing material. Sc-SWCNTs were deposited via dielectrophoresis (DEP) between interdigitated gold electrodes patterned on a 2 mm X 2 mm Si/SiO<sub>2</sub> wafer. Scanning electron microscopy (SEM) characterization of the device surface showed dense and interconnected networks formed by sc-SWCNTs, and UV-vis-NIR absorption spectroscopy of the sc-SWCNT sample showed no M<sub>11</sub> peak, confirming the high purity semiconducting content in the sc-SWCNT (Figure S2). Three approaches for the transferrin detection were evaluated in order to obtain the best transferrin sensing results. The first approach was using bare sc-SWCNTs for transferrin detection as proteins can bind to bare SWCNTs nonspecifically, changing the device characteristics.<sup>18, 40</sup> Fluorescent images taken before and after exposing sc-SWCNT to Alexa Fluor 647 conjugated transferrin demonstrated the nonspecific binding of transferrin on bare sc-SWCNTs, as red fluorescent became observable on the device surface after the addition of transferrin (Figure S3). To test for the transferrin sensing capability of bare sc-SWCNT FET

devices, a series of transferrin solutions with increasing concentrations were added to the sc-SWCNT FET devices for a 2-min incubation. FET transfer characteristics were recorded after each incubation and then analyzed to investigate the sensing performance and the sensing mechanism of the devices as FET transfer characteristics can provide more information regarding the interaction between the analyte and the CNTs than chemiresistor-mode measurements. All FET measurements were taken in nanopure water to eliminate any impact on the sensing results caused by having different ionic strengths. The calibration curve was constructed by plotting the relative response (R) at  $-0.5 \text{ V}_g$  against concentrations of transferrin on a logarithmic scale (Figure 2). FET transfer characteristics showed a decrease in the ON state current as transferrin being absorbed on sc-SWCNTs nonspecifically. However, the calibration curve demonstrated poor dose-dependent responses, and the sensitivity was significantly limited by the large device-to-device variability due to the uncontrollable amount of protein binding to each device. Furthermore, the large variance in each device may render low reliability of the sensing results, which can result in serious problems in clinical practices.

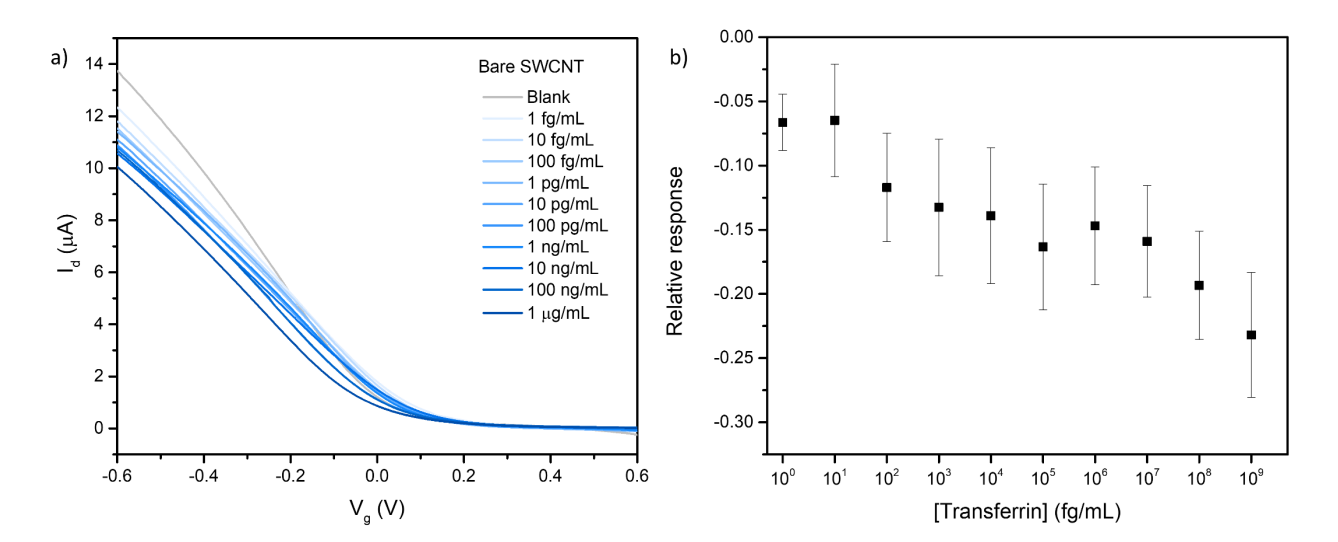


**Figure 2.** Detection of transferrin using bare SWCNT FET devices. a) FET characteristic curve of bare SWCNT FET devices upon exposure to increasing concentration of transferrin. b) Calibration plot for transferrin detection using bare SWCNT FET devices. All data points in the calibration plot are Mean  $\pm$  SD (n = 5 devices).

In order to improve the reliability, we introduced specificity to the transferrin sensor by functionalizing Tf-ab on the sc-SWCNT FET device via EDC/NHS coupling. In this case, the detection of transferrin relies upon the specific interaction between transferrin and Tf-ab near the sc-SWCNT surface. The successful integration of Tf-ab on sc-SWCNT was characterized using X-ray photoelectron spectroscopy (Figure S4), scanning electron microscopy (Figure S5), atomic force microscopy (Figure S6) and fluorescent microscopy (Figure S7). The height profiles indicated about 10 nm increase in height after the attachment of Tf-ab. Moreover, Raman spectroscopy revealed a diameter dependent functionalization of Tf-ab on sc-SWCNTs (Figure S8). Figure 3a shows the FET transfer characteristic (I-V<sub>g</sub>) curves of the Tf-ab functionalized FET device upon exposure to recombinant transferrin at varying concentrations. The threshold voltage shifted toward less negative values with increasing concentration of transferrin, which can be attributed to the introduction of negatively charged transferrin (pI ranges from 5.4 to 6.2)<sup>42</sup> near the sc-SWCNT surface, thus p-doping the SWCNTs.<sup>41</sup> The sensing performance of the Tf-ab functionalized sc-SWCNT FET sensor was then evaluated by plotting the calibration curve (Figure 3b, black). The limit of detection of the sensor was determined to be 0.01 fg/mL, suggesting an ultrasensitivity toward transferrin. The dynamic range (linear region) of the sensor was 10 fg/mL to 1 pg/mL and the calibration sensitivity, which is defined as the slope of the linear region of the calibration curve, was determined to be 0.06. While Tf-ab functionalized sc-SWCNT FET sensor demonstrated ultrasensitivity toward transferrin, this type of sensor also suffered from quick saturation at around 1 pg/mL of transferrin due to the limited binding sites available on the Tf-ab functionalized sc-SWCNTs. It led us to the third approach where the gate electrode was replaced by a gold electrode, which provided a 2 mm diameter gold disk for binding target analyte. In this configuration, instead of altering the chemical environment of SWCNT surfaces, the transferrin was being absorbed on the gold surface of the gold disk electrode, and the capacitance in the gate/electrolyte interface

is changed through modulation on the gate electrode, therefore changing the total capacitance between the gate and the semiconducting channels, inducing characteristic changes of the devices. Figure 3c showed an increase in the ON state current with transferrin absorbing on the Au surface, and the calibration curve, constructed the same way as previously described, indicated a limit of detection at 10 fg/mL and a dynamic range from 10 pg/mL to 10 ng/mL with a calibration sensitivity of 0.15 (Figure 3b, navy).

The capacitance change in the gate/electrolyte interface during transferrin detection was monitored using non-faradaic EIS. Non-faradaic EIS, which is performed without a redox probe, measures the impedance upon analyte binding to the gold surface by charging and discharging the double-layer capacitance, therefore eliminates the effect of charge transfer resistance (Rct). 46-47 A decrease in the imaginary impedance was observed in the Nyquist plot, suggesting an increasing double-layer capacitance as higher concentrations of transferrin being absorbed on the Au electrode (Figure S9). 47 Bode plot (Figure 3d) also showed a decrease in the overall impedance with increasing concentrations of transferrin in the frequency range where capacitive response was dominant, indicated by the phase angle around -85°. These results can be explained as more positively charged transferrin molecules bind to the gold surface, more charges were stored within the double layer, increasing the double-layer capacitance, which lead to the decrease in the overall impedance. 48 This increase in the gate capacitance with higher concentrations of transferrin consequently also induced the increase in transconductance (gm) of the FET characteristics (Figure S10), 49 which was observable as the increasing ON state current in the I-Vg curves.

Figure 3b compares the sensing performances of the Tf-ab-SWCNT and Au electrode approach for the detection of transferrin. Tf-ab functionalized sc-SWCNT FET devices exhibited ultrasensitivity at a limit of detection of 0.01 fg/mL while the Au electrode approach showed evident response toward transferrin at 10 fg/mL. The lower limit of detection of Tf-ab-SWCNT

approach is consistent with the lower dissociation constant of the binding between transferrin and Tf-ab (18 fg/mL for Tf-ab and 202 pg/mL for Au electrode), which corresponds to the concentration at half-maximum response. However, transferrin sensing with Au electrode outperformed the Tf-ab-SWCNT approach in terms of dynamic range of the sensor and its calibration sensitivity, as Au electrode provided a larger sensing area, hence more available binding sites for transferrin molecules. Therefore, various factors, such as transferrin concentration, sensitivity and specificity requirements, need to be considered before choosing the optimal transferrin sensing method.

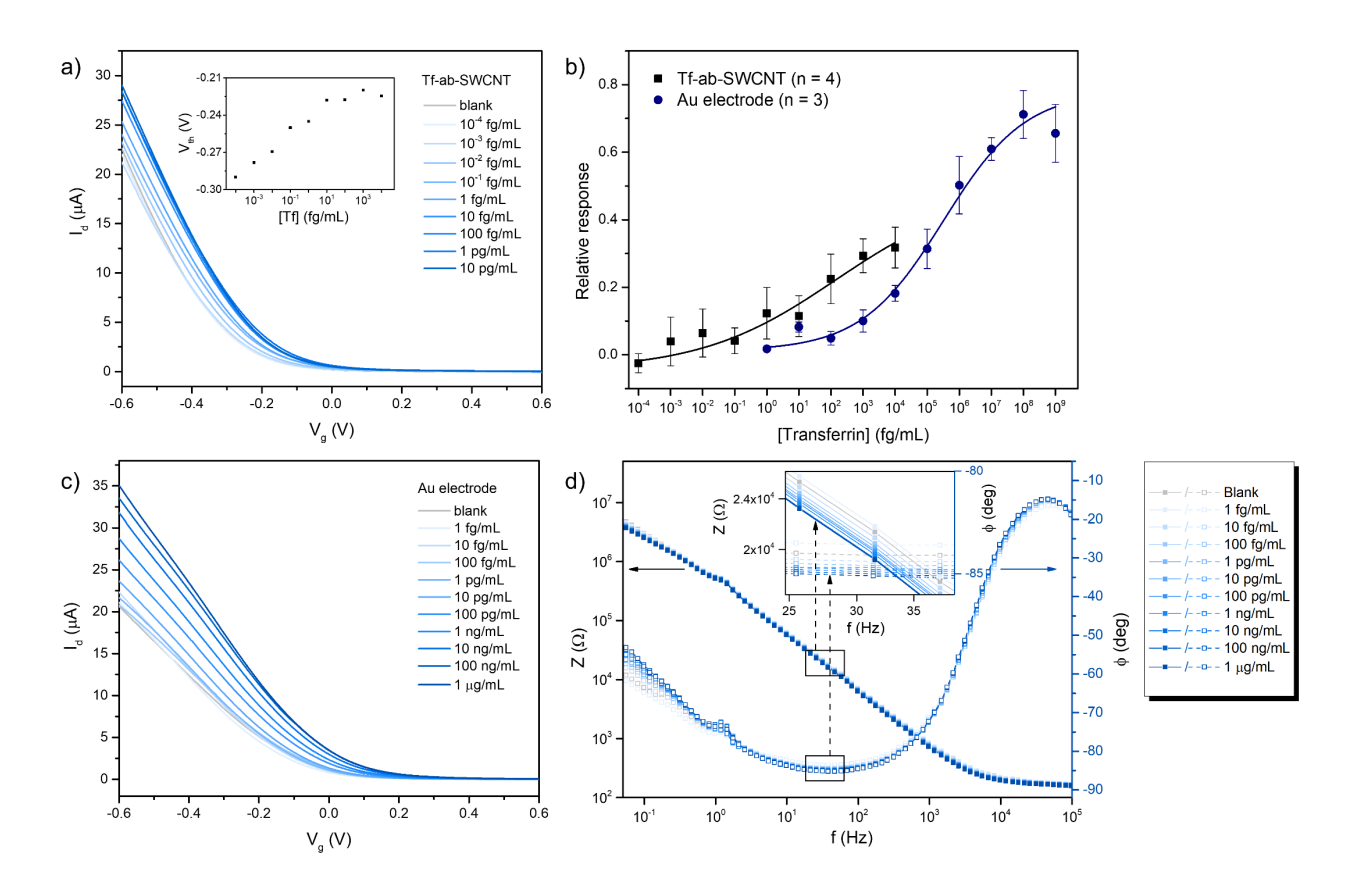
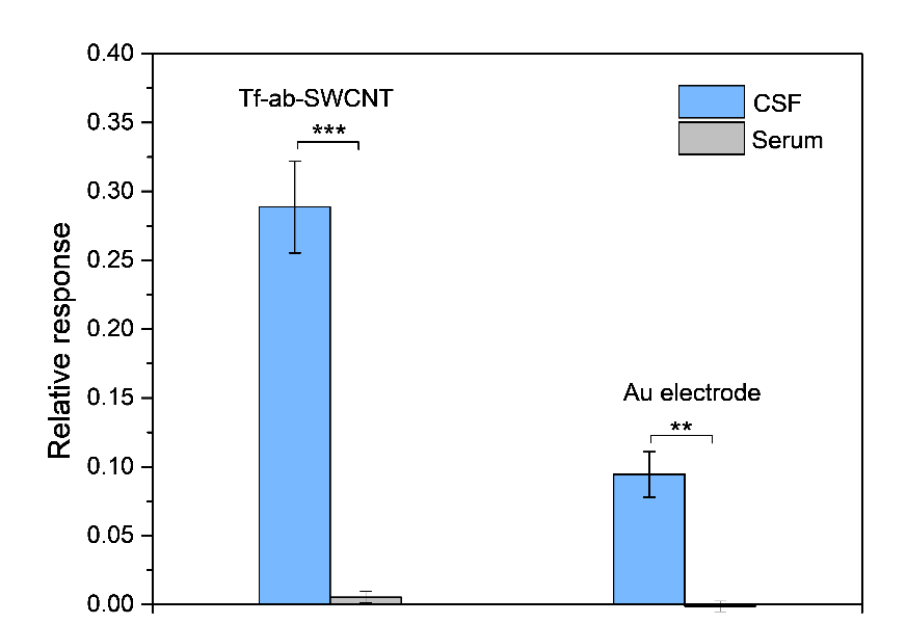


Figure 3. Detection of recombinant transferrin using sc-SWCNT FET devices. a) FET characteristic curves of Tf-ab functionalized SWCNT (Tf-ab-SWCNT) FET device upon exposure to increasing concentration of recombinant transferrin. Inset shows the threshold voltage shift. b) Calibration plot for transferrin detection using Tf-ab-SWCNT approach and Au electrode approach. Results are Mean ± SD. The number (n) of devices used for calculation are indicated in the parenthesis in the legend. c) FET characteristic curves of sc-SWCNT FET device with increasing concentration of recombinant transferrin absorbing on the Au gate electrode. d) Bode plot of EIS measurement of the Au electrode upon transferrin binding. Inset shows a zoom-in view of the impedance of the Au electrode surface in the capacitive response region.

Our 3-step strategy for  $\beta$ 2-Tf detection was then applied to differentiate samples of CSF and serum. Transferrin component of both CSF and serum were studied using electrophoresis and Western blot (Figure S11). CSF, which contains  $\beta$ 2-Tf, showed two transferrin bands with the leading band

representing β2-Tf. Serum, on the other hand, only yielded one transferrin band due to the lack of β2-Tf. Four pairs of CSF and serum samples were tested following the 3-step method, and the β2-Tf detection in step 3 was carried out using both Tf-ab-SWCNTs and Au electrode approach. Both detection methods achieved the differentiation between CSF and serum samples, but Tf-ab functionalized sc-SWCNT FET devices displayed better sensing performance by yielding higher signal and more reliable results due to the ultrasensitivity in the lower transferrin concentration range. However, as previously mentioned, the Au electrode approach might outperform the Tf-ab-SWCNT approach with higher transferrin concentration present in the sample. Therefore, the selection of the sensing approach in step 3 should depend on the transferrin concentration.



**Figure 4.** β2-Tf detection in CSF (blue) and serum (grey) using Tf-ab-SWCNT FET devices and Au electrode approach. Results are mean  $\pm$  SEM. The number (n) of devices tested for each sample was summarized in Table S2. (ANOVA; \*\*, p<0.01; \*\*\*, p<0.001)

#### 4. CONCLUSION

In summary, we presented a 3-step strategy for rapid β2-Tf detection in body fluids, which is required in clinical diagnostic of CSF leakage after traumatic brain injury (TBI) or surgical procedures. The 3-step strategy includes two steps of affinity columns for separating β2-Tf from other proteins present in the fluid sample, and a third step using high purity sc-SWCNT FET devices for β2-Tf detection. Both Tf-ab-SWCNT and Au electrode approach in step 3 have shown their capability of \( \beta 2\)-Tf detection with high sensitivity and reliability. Tf-ab functionalized sc-SWCNT FET devices exhibited ultrasensitivity at a limit of detection of 0.01 fg/mL with a dynamic range of 10 fg/mL to 1 pg/mL, hence suitable for the ultrasensitive β2-Tf detection in sub-pg/mL range. On the other hand, transferrin sensing with Au electrode outperformed the Tfab-SWCNT approach in the ng/mL transferrin range with wider dynamic range and higher calibration sensitivity. By applying the 3-step strategy to body fluids, we have successfully differentiated CSF (positive) and serum (negative) samples using both Tf-ab-SWCNT and Au electrode approach. Compared to current methods for CSF leak diagnosis, such as electrophoresis and imaging methods, our 3-step strategy is capable of offering high quality CSF leak detection with a short turnaround time (around 1 hour), easy instrument access and simple operations, which could potentially benefit patient care for TBI patients and other people in need. Furthermore, the high-purity sc-SWCNT based FET biosensing chip utilized in step 3 can be incorporated into a portable electronic unit with intuitive readout, similar to a breathalyzer.<sup>51-52</sup> Therefore, the miniaturizability as well as the versatility of our sensing platform could also open opportunities for point-of-care applications for other disease-related protein detection.

#### ASSOCIATE CONTENTS

# **Supporting Information**

ELISA restuls, XPS, Raman, SEM, AFM and fluorescence micrscopy characterizations of the functionalized sc-SWCNT devices, EIS study of the gold-disk electrode and Western blot of serum and CSF samples supplied as Supporting Information.

#### **ACKNOWLEDGEMENTS**

The authors would like to acknowledge Dr. Daniel Lamont from the Nanoscale Fabrication and Characterization Facility at University of Pittsburgh for obtaining the scanning electron microscopy image presented in Figure S2.

The work was supported by the National Science Foundation under Grant No. 2003302. The XplorA Raman-AFM/TERS system was purchased via Defense University Research Instrumentation Program (DURIP) grant from the Office of Naval Research, ONR (N000141410765).

#### **AUTHOR INFORMATION**

## **Corresponding Author**

**Alexander Star** – Department of Chemistry, University of Pittsburgh, Pittsburgh, Pennsylvania 15260, United States; Department of Bioengineering, University of Pittsburgh, Pittsburgh, Pennsylvania 15261, United States; orcid.org/0000-0001-7863-5987; Email: <a href="mailto:astar@pitt.edu">astar@pitt.edu</a>

#### **Authors**

Wenting Shao – Department of Chemistry, University of Pittsburgh, Pittsburgh, Pennsylvania 15260, United States; orcid.org/0000-0002-5615-9980

**Galina V. Shurin** – Department of Pathology, University of Pittsburgh Medical Center, Pittsburgh, Pennsylvania 15260, United States

**Xiaoyun He** – Department of Chemistry, University of Pittsburgh, Pittsburgh, Pennsylvania 15260, United States; orcid.org/0000-0001-7313-4585

**Zidao Zeng** – Department of Chemistry, University of Pittsburgh, Pittsburgh, Pennsylvania 15260, United States

**Michael R. Shurin** – Department of Pathology, University of Pittsburgh Medical Center, Pittsburgh, Pennsylvania 15260, United States; orcid.org/0000-0002-6570-7395

## **Notes**

The authors declare no competing interests.

#### REFERENCES

- 1. Schlosser, R. J.; Bolger, W. E., Nasal Cerebrospinal Fluid Leaks: Critical Review and Surgical Considerations. *Laryngoscope* **2004**, *114*, 255–265.
- 2. Banks, C. A.; Palmer, J. N.; Chiu, A. G.; O'Malley, B. W., Jr.; Woodworth, B. A.; Kennedy, D. W., Endoscopic Closure of CSF Rhinorrhea: 193 Cases Over 21 Years.

  Otolaryngol. Head Neck Surg. 2009, 140, 826–833.
- 3. Mantur, M.; Lukaszewicz-Zajac, M.; Mroczko, B.; Kulakowska, A.; Ganslandt, O.; Kemona, H.; Szmitkowski, M.; Drozdowski, W.; Zimmermann, R.; Kornhuber, J.; Lewczuk, P.,

- Cerebrospinal Fluid Leakage-Reliable Diagnostic Methods. *Clin. Chim. Acta* **2011**, *412*, 837–840.
- 4. Oakley, G. M.; Alt, J. A.; Schlosser, R. J.; Harvey, R. J.; Orlandi, R. R., Diagnosis of Cerebrospinal Fluid Rhinorrhea: An Evidence-Based Review with Recommendations. *Int. Forum Allergy Rhinol.* **2016**, *6*, 8–16.
- 5. Macedo, M. F.; de Sousa, M., Transferrin and the Transferrin Receptor: Of Magic Bullets and Other Concerns. *Inflamm. Allergy Drug Targets* **2008**, *7*, 41–52.
- 6. Arrer, E.; Oberascher, G.; Gibitz, H.-J., Protein Distribution in the Human Perilymph: A Comparative Study between Perilymph (Post Mortem), CSF and Blood Serum. *Acta Otolaryngol.* **1988**, *106*, 117–123.
- 7. Schnabel, C.; Martino, E. D.; Gilsbach, J. M.; Riediger, D.; Gressner, A. M.; Kunz, D., Comparison of β2-Transferrin and β-Trace Protein for Detection of Cerebrospinal Fluid in Nasal and Ear Fluids. *Clin. Chem.* **2004**, *50*, 661–663.
- 8. Brown, K. J.; Vanderver, A.; Hoffman, E. P.; Schiffmann, R.; Hathout, Y., Characterization of Transferrin Glycopeptide Structures in Human Cerebrospinal Fluid. *Int. J. Mass Spectrom.* **2012**, *312*, 97–106.
- 9. Normansell, D. E.; Stacy, E. K.; Booker, C. F.; Butler, T. Z., Detection of Beta-2 Transferrin in Otorrhea and Rhinorrhea in a Routine Clinical Laboratory Setting. *Clin. Diagn. Lab. Immunol.* **1994**, *1*, 68–70.
- 10. Anani, W. Q.; Ojerholm, E.; Shurin, M. R., Resolving Transferrin Isoforms via Agarose Gel Electrophoresis. *Lab. Med.* **2015**, *46*, 26–33.

- 11. Kumar, S.; Tripathy, S.; Jyoti, A.; Singh, S. G., Recent Advances in Biosensors for Diagnosis and Detection of Sepsis: A Comprehensive Review. *Biosens. Bioelectron.* **2019**, *124 125*, 205–215.
- 12. Florea, A.; Melinte, G.; Simon, I.; Cristea, C., Electrochemical Biosensors as Potential Diagnostic Devices for Autoimmune Diseases. *Biosensors (Basel)* **2019**, *9*, 38.
- 13. Gupta, S.; Kaushal, A.; Kumar, A.; Kumar, D., Recent Advances in Biosensors for Diagnosis of Celiac Disease: A Review. *Biotechnol. Bioeng.* **2019**, *116*, 444–451.
- 14. Shandilya, R.; Bhargava, A.; Bunkar, N.; Tiwari, R.; Goryacheva, I. Y.; Mishra, P. K., Nanobiosensors: Point-of-Care Approaches for Cancer Diagnostics. *Biosens. Bioelectron.* **2019**, *130*, 147–165.
- 15. Farzin, L.; Shamsipur, M.; Samandari, L.; Sheibani, S., HIV Biosensors for Early Diagnosis of Infection: The Intertwine of Nanotechnology with Sensing Strategies. *Talanta* **2020**, *206*, 120201.
- 16. Carneiro, P.; Morais, S.; do Carmo Pereira, M., Biosensors on the Road to Early Diagnostic and Surveillance of Alzheimer's Disease. *Talanta* **2020**, *211*, 120700.
- 17. Shao, W.; Shurin, M. R.; Wheeler, S. E.; He, X.; Star, A., Rapid Detection of SARS-CoV-2 Antigens Using High-Purity Semiconducting Single-Walled Carbon Nanotube-Based Field-Effect Transistors. *ACS Appl. Mater. Interfaces* **2021**, *13*, 10321–10327.
- 18. Allen, B. L.; Kichambare, P. D.; Star, A., Carbon Nanotube Field-Effect-Transistor-Based Biosensors. *Adv. Mater.* **2007**, *19*, 1439–1451.
- 19. De Volder, M. F. L.; Tawfick, S. H.; Baughman, R. H.; Hart, A. J., Carbon Nanotubes: Present and Future Commercial Applications. *Science* **2013**, *339*.

- 20. Lee, C.-S.; Kim, J. S.; Kim, T. H., A Chemodosimeter-Modified Carbon Nanotube-Field Effect Transistor: Toward a Highly Selective and Sensitive Electrical Sensing Platform. *RSC Adv.* **2019**, *9*, 28414–28420.
- 21. Odom, T. W.; Huang, J.-L.; Kim, P.; Lieber, C. M., Atomic Structure and Electronic Properties of Single-Walled Carbon Nanotubes. *Nature* **1998**, *391*, 62–64.
- 22. Ding, J.; Li, Z.; Lefebvre, J.; Cheng, F.; Dubey, G.; Zou, S.; Finnie, P.; Hrdina, A.; Scoles, L.; Lopinski, G. P.; Kingston, C. T.; Simard, B.; Malenfant, P. R., Enrichment of Large-Diameter Semiconducting SWCNTs by Polyfluorene Extraction for High Network Density Thin Film Transistors. *Nanoscale* **2014**, *6*, 2328–2339.
- 23. Lefebvre, J.; Ding, J.; Li, Z.; Finnie, P.; Lopinski, G.; Malenfant, P. R. L., High-Purity Semiconducting Single-Walled Carbon Nanotubes: A Key Enabling Material in Emerging Electronics. *Acc. Chem. Res.* **2017**, *50*, 2479–2486.
- 24. Zhou, C.; Zhao, J.; Ye, J.; Tange, M.; Zhang, X.; Xu, W.; Zhang, K.; Okazaki, T.; Cui, Z., Printed Thin-Film Transistors And NO<sub>2</sub> Gas Sensors Based on Sorted Semiconducting Carbon Nanotubes by Isoindigo-Based Copolymer. *Carbon* **2016**, *108*, 372–380.
- 25. Xiao, M.; Liang, S.; Han, J.; Zhong, D.; Liu, J.; Zhang, Z.; Peng, L., Batch Fabrication of Ultrasensitive Carbon Nanotube Hydrogen Sensors with Sub-ppm Detection Limit. *ACS Sens*. **2018**, *3*, 749–756.
- 26. Li, Z.; Ding, J.; Guo, C.; Lefebvre, J.; Malenfant, P. R. L., Decomposable s-Tetrazine Copolymer Enables Single Walled Carbon Nanotube Thin Film Transistors and Sensors with Improved Sensitivity. *Adv. Funct. Mater.* **2018**, *28*, 1705568.

- 27. Jeon, J. Y.; Kang, B. C.; Byun, Y. T.; Ha, T. J., High-Performance Gas Sensors Based on Single-Wall Carbon Nanotube Random Networks For The Detection of Nitric Oxide Down to the Ppb-Level. *Nanoscale* **2019**, *11*, 1587–1594.
- Zhang, H.; Xiang, L.; Yang, Y.; Xiao, M.; Han, J.; Ding, L.; Zhang, Z.; Hu, Y.; Peng, L. M., High-Performance Carbon Nanotube Complementary Electronics and Integrated Sensor Systems on Ultrathin Plastic Foil. ACS Nano 2018, 12, 2773–2779.
- 29. Liu, Y.; Wei, N.; Zhao, Q.; Zhang, D.; Wang, S.; Peng, L. M., Room Temperature Infrared Imaging Sensors Based on Highly Purified Semiconducting Carbon Nanotubes. *Nanoscale* **2015**, *7*, 6805–6812.
- 30. Zheng, H. Y.; Alsager, O. A.; Zhu, B.; Travas-Sejdic, J.; Hodgkiss, J. M.; Plank, N. O. V., Electrostatic Gating in Carbon Nanotube Aptasensors. *Nanoscale* **2016**, *8*, 13659–13668.
- 31. Thanihaichelvan, M.; Browning, L. A.; Dierkes, M. P.; Reyes, R. M.; Kralicek, A. V.; Carraher, C.; Marlow, C. A.; Plank, N. O. V., Metallic-Semiconducting Junctions Create Sensing Hot-Spots in Carbon Nanotube FET Aptasensors Near Percolation. *Biosens. Bioelectron.* **2019**, *130*, 408–413.
- 32. Xu, X.; Clement, P.; Eklof-Osterberg, J.; Kelley-Loughnane, N.; Moth-Poulsen, K.; Chavez, J. L.; Palma, M., Reconfigurable Carbon Nanotube Multiplexed Sensing Devices. *Nano Lett.* **2018**, *18*, 4130–4135.
- 33. Sorgenfrei, S.; Chiu, C. Y.; Gonzalez, R. L., Jr.; Yu, Y. J.; Kim, P.; Nuckolls, C.; Shepard, K. L., Label-Free Single-Molecule Detection of DNA-Hybridization Kinetics with a Carbon Nanotube Field-Effect Transistor. *Nat. Nanotechnol.* **2011**, *6*, 126–132.
- 34. Filipiak, M. S.; Rother, M.; Andoy, N. M.; Knudsen, A. C.; Grimm, S.; Bachran, C.; Swee, L. K.; Zaumseil, J.; Tarasov, A., Highly Sensitive, Selective and Label-Free Protein

- Detection in Physiological Solutions using Carbon Nanotube Transistors with Nanobody Receptors. *Sens. Actuators B Chem.* **2018,** *255*, 1507–1516.
- 35. Hatada, M.; Tran, T. T.; Tsugawa, W.; Sode, K.; Mulchandani, A., Affinity Sensor for Haemoglobin A1c Based on Single-Walled Carbon Nanotube Field-Effect Transistor and Fructosyl Amino Acid Binding Protein. *Biosens. Bioelectron.* **2019**, *129*, 254–259.
- 36. Shao, W.; Burkert, S. C.; White, D. L.; Scott, V. L.; Ding, J.; Li, Z.; Ouyang, J.; Lapointe, F.; Malenfant, P. R. L.; Islam, K.; Star, A., Probing Ca<sup>2+</sup>-Induced Conformational Change of Calmodulin with Gold Nanoparticle-Decorated Single-Walled Carbon Nanotube Field-Effect Transistors. *Nanoscale* **2019**, *11*, 13397–13406.
- 37. Ochoa, E. L. M.; Bangham, A. D., N-Acetylneuraminic Acid Molecules as Possible Serotonin Binding Sites. *J. Neurochem.* **1976,** *26*, 1193–1198.
- 38. Yodoshi, M.; Ikuta, T.; Mouri, Y.; Suzuki, S., Specific Extraction of Sialic-Acid-Containing Glycans and Glycopeptides using Serotonin-bonded Silica. *Anal. Sci.* **2010**, *26*, 75–81.
- 39. Meininger, M.; Stepath, M.; Hennig, R.; Cajic, S.; Rapp, E.; Rotering, H.; Wolff, M. W.; Reichl, U., Sialic Acid-Specific Affinity Chromatography for the Separation of Erythropoietin Glycoforms using Serotonin as a Ligand. *J. Chromatogr. B* **2016**, *1012–1013*, 193–203.
- 40. Calvaresi, M.; Zerbetto, F., The Devil and Holy Water: Protein and Carbon Nanotube Hybrids. *Acc. Chem. Res.* **2013**, *46*, 2454–2463.
- 41. Heller, I.; Janssens, A. M.; Mannik, J.; Minot, E. D.; Lemay, S. G.; Dekker, C., Identifying the Mechanism of Biosensing with Carbon Nanotube Transistors. *Nano Lett.* **2008,** *8*, 591–595.

- 42. Grange, P. a.; Mouricout, M. a., Transferrin Associated with the Porcine Intestinal Mucosa Is a Receptor Specific for K88ab Fimbriae of *Escherichia coli*. *Infect. Immun.* **1996,** *64*, 606–610.
- 43. Mulla, M. Y.; Tuccori, E.; Magliulo, M.; Lattanzi, G.; Palazzo, G.; Persaud, K.; Torsi, L., Capacitance-Modulated Transistor Detects Odorant Binding Protein Chiral Interactions. *Nat. Commun.* **2015**, *6*, 6010.
- 44. Macchia, E.; Manoli, K.; Holzer, B.; Di Franco, C.; Ghittorelli, M.; Torricelli, F.; Alberga, D.; Mangiatordi, G. F.; Palazzo, G.; Scamarcio, G.; Torsi, L., Single-Molecule Detection with a Millimetre-Sized Transistor. *Nat. Commun.* **2018**, *9*, 3223.
- 45. Nguyen, T. T. K.; Tran, H. V.; Vu, T. T.; Reisberg, S.; Noel, V.; Mattana, G.; Pham, M. C.; Piro, B., Peptide-Modified Electrolyte-Gated Organic Field Effect Transistor. Application to Cu<sup>2+</sup> Detection. *Biosens. Bioelectron.* **2019**, *127*, 118–125.
- 46. Kazemi, S. H.; Shanehsaz, M.; Ghaemmaghami, M., Non-Faradaic Electrochemical Impedance Spectroscopy as a Reliable and Facile Method: Determination of the Potassium Ion Concentration Using a Guanine Rich Aptasensor. *Mater. Sci. Eng. C* **2015**, *52*, 151–154.
- 47. Tanak, A. S.; Jagannath, B.; Tamrakar, Y.; Muthukumar, S.; Prasad, S., Non-Faradaic Electrochemical Impedimetric Profiling of Procalcitonin and C-Reactive Protein as a Dual Marker Biosensor for Early Sepsis Detection. *Anal. Chim. Acta X* **2019**, *3*, 100029.
- 48. Stevenson, H.; Radha Shanmugam, N.; Paneer Selvam, A.; Prasad, S., The Anatomy of a Nonfaradaic Electrochemical Biosensor. *SLAS Technol.* **2018**, *23*, 5–15.
- 49. Diacci, C.; Berto, M.; Di Lauro, M.; Bianchini, E.; Pinti, M.; Simon, D. T.; Biscarini, F.; Bortolotti, C. A., Label-Free Detection of Interleukin-6 Using Electrolyte Gated Organic Field Effect Transistors. *Biointerphases* **2017**, *12*, 05F401.

- 50. Zhu, D. M.; Dustin, M. L.; Cairo, C. W.; Golan, D. E., Analysis of Two-Dimensional Dissociation Constant of Laterally Mobile Cell Adhesion Molecules. *Biophys. J.* **2007**, *92*, 1022–1034.
- 51. Hwang, S. I.; Franconi, N. G.; Rothfuss, M. A.; Bocan, K. N.; Bian, L.; White, D. L.; Burkert, S. C.; Euler, R. W.; Sopher, B. J.; Vinay, M. L.; Sejdic, E.; Star, A., Tetrahydrocannabinol Detection Using Semiconductor-Enriched Single-Walled Carbon Nanotube Chemiresistors. *ACS Sens.* **2019**, *4*, 2084–2093.
- 52. Hwang, S. I.; Chen, H. Y.; Fenk, C.; Rothfuss, M. A.; Bocan, K. N.; Franconi, N. G.; Morgan, G. J.; White, D. L.; Burkert, S. C.; Ellis, J. E.; Vinay, M. L.; Rometo, D. A.; Finegold, D. N.; Sejdic, E.; Cho, S. K.; Star, A., Breath Acetone Sensing Based on Single-Walled Carbon Nanotube-Titanium Dioxide Hybrids Enabled by a Custom-Built Dehumidifier. *ACS Sens.* **2021**, *6*, 871–880.

# TOC graphic

